Quantification of Retinal Ganglion Cell Morphology in Human Glaucomatous Eyes

Zhuolin Liu,[1] Osamah Saeedi,[2] Furu Zhang,[1] Ricardo Villanueva,[2] Samuel Asanad,[2] Anant Agrawal,[1] and Daniel X. Hammer[1]

[1]Center for Devices and Radiological Health (CDRH), U.S. Food and Drug Administration, Silver Spring, Maryland, United States
[2]Department of Ophthalmology and Visual Sciences, University of Maryland School of Medicine, Baltimore Maryland, United States

Correspondence: Zhuolin Liu, Center for Devices and Radiological Health (CDRH), U.S. Food and Drug Administration, 10903 New Hampshire Ave, Silver Spring, MD 20993, USA; zhuolin.liu@fda.hhs.gov.

ZL and OS are joint first authors.

Received: November 9, 2020
Accepted: February 26, 2021
Published: March 24, 2021

Citation: Liu Z, Saeedi O, Zhang F, et al. Quantification of retinal ganglion cell morphology in human glaucomatous eyes. *Invest Ophthalmol Vis Sci.* 2021;62(3):34. https://doi.org/10.1167/iovs.62.3.34

Purpose. To characterize retinal ganglion cell morphological changes in patients with primary open-angle glaucoma associated with hemifield defect (HD) using adaptive optics–optical coherence tomography (AO-OCT).

Methods. Six patients with early to moderate primary open-angle glaucoma with an average age of 58 years associated with HD and six age-matched healthy controls with an average age of 61 years were included. All participants underwent in vivo retinal ganglion cell (RGC) imaging at six primary locations across the macula with AO-OCT. Ganglion cell layer (GCL) somas were manually counted, and morphological parameters of GCL soma density, size, and symmetry were calculated. RGC cellular characteristics were correlated with functional visual field measurements.

Results. GCL soma density was 12,799 ± 7747 cells/mm^2, 9370 ± 5572 cells/mm^2, and 2134 ± 1494 cells/mm^2 at 3°, 6°, and 12°, respectively, in glaucoma patients compared with 25,058 ± 4649 cells/mm^2, 15,551 ± 2301 cells/mm^2, and 3891 ± 1105 cells/mm^2 ($P <$ 0.05 for all locations) at the corresponding retinal locations in healthy participants. Mean soma diameter was significantly larger in glaucoma patients (14.20 ± 2.30 µm) compared with the health controls (12.32 ± 1.94 µm, $P < 0.05$ for all locations); symmetry was 0.36 ± 0.32 and 0.86 ± 0.13 in glaucoma and control cohorts, respectively.

Conclusions. Glaucoma patients had lower GCL soma density and symmetry, greater soma size, and increased variation of GCL soma reflectance compared with age-matched control subjects. The morphological changes corresponded with HD, and the cellular level structural loss correlated with visual function loss in glaucoma. AO-based morphological parameters could be potential sensitive biomarkers for glaucoma.

Keywords: Primary open-angle glaucoma, adaptive optics, optical coherence tomography, retinal ganglion cell

Glaucoma is an optic neuropathy that is a leading cause of irreversible blindness worldwide. By 2040 more than 100 million people are expected to suffer from the disease.[1] Vision loss in glaucoma is caused primarily by progressive loss and degeneration of retinal ganglion cell (RGC) axons and their somas,[2] losing the capacity to convey visual information to the brain. The initiating injury to RGCs and axons is believed to occur within the optic nerve head.[3] Primary open-angle glaucoma (POAG) often manifests without intraocular pressure (IOP) elevation, a primary risk factor of the disease. Although glaucoma has been extensively studied, the mechanisms and course of the disease are still incompletely understood.[3]

The current standard of care for glaucoma includes visual field (VF) tests to detect functional loss and optical coherence tomography (OCT) to detect changes in peripapillary retinal nerve fiber layer (RNFL) thickness. These tests have limitations that result in potential delays in diagnosis and treatment. VF tests are useful for diagnosis and monitoring of individuals with moderate to severe glaucoma but are subjective and can be highly variable.[4–6] OCT is objective and can be used for early glaucoma diagnosis but in more advanced glaucoma RNFL thickness measurements have a "floor effect" where progression cannot be further tracked when the RNFL has thinned below a certain value.[5,7] Currently, glaucoma treatment relies on reduction of IOP with medication, laser, or surgery. Potential future neuroprotective strategies have focused on mitigating risk factors, such as decreased neurotrophin support, glutamate-associated excitotoxicity, hypoperfusion, and vasospasm, associated with RGC loss.[8,9] Because glaucoma is a slow progressive disease, a key hurdle to neuroprotection trials is the lack of highly sensitive and reliable biomarkers both for disease progression (i.e., to determine when to begin treatment) and therapeutic efficacy (i.e., to determine how well an individual responds to treatment), which results in the need for lengthy and costly studies.[10] Hence, there is a critical need for new surrogate

clinical endpoints that are intrinsically related to disease pathogenesis.

Although clinical diagnosis relies on relatively coarse measurements such as perimetry and RNFL thickness, studies of disease etiology and mechanisms benefit from the cellular-level detail obtained with histological and in vivo experimental animal studies. Such studies have shown that RGC apoptosis occurs early and persists throughout glaucoma progression.[3,11–16] However, questions remain regarding the characteristics and nature of cellular changes that take place during cell death in living human glaucomatous eyes (Do RGCs shrink or enlarge into voids left after their nearest neighbors die?),[3] the susceptibility of ganglion cell types to disease (Are midget and parasol RGCs affected equivalently by glaucoma?),[3] the sequence of structural changes (Does RGC soma loss precede their dendritic degeneration?),[17] the regional characteristics of progression (Does RGC cell loss follow functional losses—preceding peripheral to central, or is this disease characteristic attributable to the higher pre-disease RGC density in more central locations?),[18] and the order and sensitivity of functional loss compared to structural changes (Can structural changes be detected prior to visual function loss?).[18] Until recently, cellular-level RGC imaging in live human subjects was not possible to help answer these questions.

Adaptive optics (AO) has enabled resolution of many cellular structures in living eyes by compensating for ocular aberrations. This technology has been primarily integrated into OCT and scanning laser ophthalmoscopy (SLO) devices.[19–23] With cellular-level resolution, AO holds great promise for improved diagnosis and treatment outcome assessment for many ocular diseases such as age-related macular degeneration, glaucoma, and others. The application of AO to glaucoma often focused on retinal structures that generated strong optical signal such as lamina cribrosa,[24,25] nerve fiber bundles,[26–30] retinal vasculature,[31] microcystic lesions in the inner nuclear layer,[32] and photoreceptors in the outer retina.[33,34] Although results were encouraging, these studies did not examine the fundamental cellular layer important to glaucoma, the ganglion cell layer (GCL). Retinal ganglion cells have proven much more difficult to resolve in living eyes because of their relative transparency and dense three-dimensional (3D) packing arrangement.[23,32,35–37] In 2017, Liu et al.[36] first demonstrated the ability to resolve the GCL soma mosaic across the macula in human subjects with healthy eyes using AO-OCT. This scientific breakthrough laid the foundation for the current study—a detailed analysis of RGC morphology in eyes with glaucoma. Although AO-OCT provides the capability to resolve RGC soma, it also operates with a relatively limited field of view (FOV) and requires significant averaging, which prevents wide-field operation. Therefore we carefully designed the current pilot study to image glaucoma subjects with early to moderate disease and known hemifield defect (HD), providing an opportunity to probe RGC structural measures at several precise macular regions of clinical structural and functional deficits (i.e., above and below the midline). The primary hypothesis being tested is that glaucoma causes specific GCL cellular changes (in density and cell diameter), which are associated with HD and detectable by AO-OCT. The study demonstrates for the first time the ability to measure RGC morphological characteristics in glaucomatous eye to begin to provide preliminary answers to long-standing questions about glaucoma etiology, mechanisms, and progression.

Methods

Participants and Initial Clinical Examination

The study protocol was approved by the Institutional Review Boards of the Food and Drug Administration (FDA) and the University of Maryland and adhered to the tenets of the Declaration of Helsinki. Written informed consent was obtained after the potential risks were explained to each participant. Six POAG patients and six age-matched healthy control subjects with an average (± standard deviation [SD]) age of 58 ± 4 and 61 ± 8 years, respectively, were enrolled. The glaucoma participants had early to moderate disease and an HD with localized VF loss (mean deviation [MD]: −3.3 dB; pattern standard deviation: 3.8 dB). All participants had open angles documented by gonioscopy and underwent standard ophthalmic examination (summarized in Supplementary Table S1) with measurement of optic disc photography and OCT (peripapillary and macula scans, Spectralis OCT; Heidelberg Engineering GmbH, Heidelberg, Germany). In addition, glaucoma participants underwent standard automated perimetry with the Humphrey Field Analyzer (Carl Zeiss Meditec Inc., Dublin, CA, USA) using both 24-2 and 10-2 SITA standard protocols. Inclusion criteria for control subjects included open angles on gonioscopy, OCT RNFL within normal limits, intraocular pressure below 21 mm Hg, healthy and symmetric neuroretinal rims, and a clinically examined cup-to-disc ratio (CDR) of 0.5 or less. Inclusion criteria for glaucoma patients included diagnosis of POAG based on the American Academy of Ophthalmology Practice Patterns[38] made by an experienced glaucoma specialist (OJS), and presence of asymmetric glaucomatous damage manifesting as visual field loss confined to one hemifield that corresponded to RNFL and GCL thinning on the opposite side. All glaucoma subjects had been seen by the same glaucoma specialist for at least three years and had completed at least six visual field tests. Their visual fields were assessed by the glaucoma specialist and noted to be reliable and consistent with prior fields. They were beyond the learning curve phase. Glaucoma severity was graded based on the Hodapp-Andersen-Parrish criteria as early, moderate, or severe based on their most recent VF test result.[39] One patient did not meet criteria for glaucoma based solely on visual field but had visual field loss with characteristic RNFL thinning and GCL thinning in the opposite hemifield. Exclusion criteria were presence of media opacity, unreliable VF results, comorbid ocular disease (e.g., diabetic retinopathy or age-related macular degeneration), prior ocular surgery other than uncomplicated cataract extraction or glaucoma surgery, or inability to fixate for standard clinical OCT. After completion of clinical testing, in vivo RGC imaging with a multimodal AO imager was performed to measure RGC density and morphological parameters of GCL soma diameter and asymmetry. If both eyes met inclusion and exclusion criteria in glaucoma patients and normal controls, the right eye was chosen for AO imaging. One glaucoma patient was imaged twice in the AO system, approximately eight months before and one month after glaucoma surgery.

In Vivo RGC Imaging With the FDA Multimodal AO Imager

The participant's eye was cyclopleged and dilated with 1% tropicamide for AO imaging. AO-OCT images were acquired

Investigative Ophthalmology & Visual Science

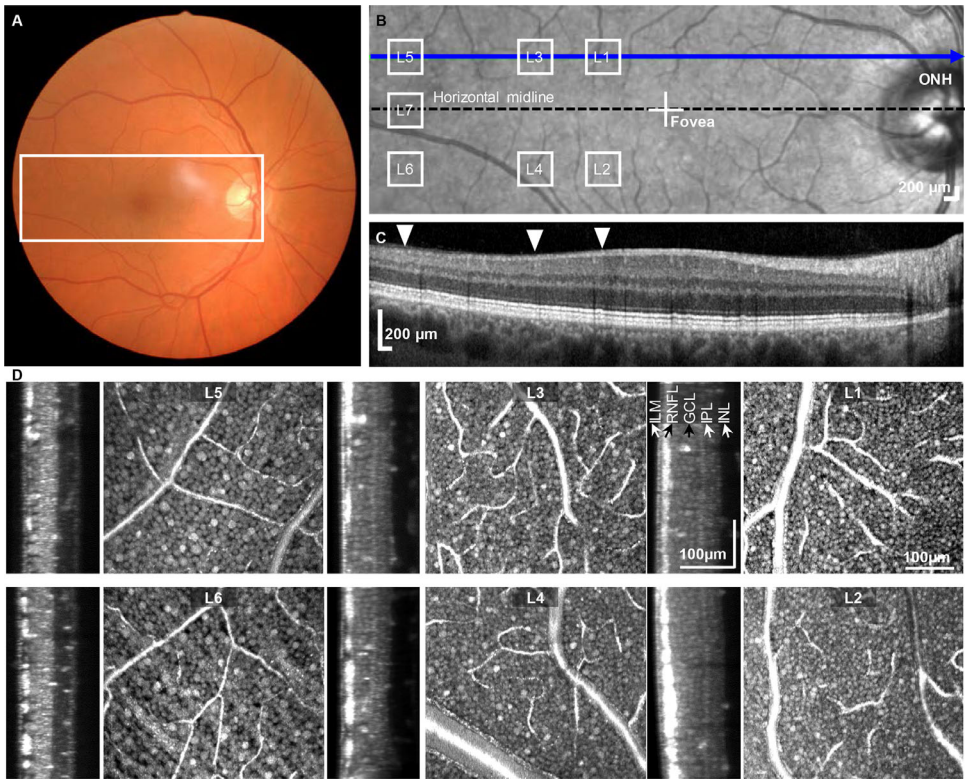

Figure 1. Images of the right eye of a 54-year-old control subject (6289). Clinical data includes (**A**) fundus photograph, (**B**) Spectralis scanning laser ophthalmoscopy, and (**C**) optical coherence tomography B-scan at 2.5° superior retina, location denoted by *blue arrow line* in (**B**). There are no signs of glaucoma, such as disc-rim thinning or RNFL defects. The *white rectangular box* in (**A**) corresponds to the same region in (**B**) and the labeled *seven white boxes* in (**B**) are the locations where our adaptive optics–optical coherence tomography (AO-OCT) data were acquired. The *white arrows* in (**C**) corresponded with the three retinal locations (*L1*, *L3*, and *L5*) in (**B**). (**D**) Representative AO-OCT B-scans of the inner retina (from ILM to INL) on the left oriented vertically for comparison of hemifield differences and en face views of a single plane at the six corresponding retinal eccentricities (*L1–L6*). ILM, inner limiting membrane; RNFL, retinal nerve fiber layer; GCL, ganglion cell layer; IPL, inner plexiform layer; INL, inner nuclear layer.

with the FDA multimodal system[40] operated at 830 nm ($\Delta\lambda$ = 60 nm) and illumination power less than 430 µW, which was within safe limits established by American National Standards Institute (ANSI).[41] System focus was set approximately at the GCL to maximize GCL soma contrast by optimizing GCL layer brightness in the real-time B-scan (cross sectional) display and sharpness of the NFL speckle patterns in the SLO channel prior to AO-OCT image collection. AO-OCT volumes were acquired on the subjects at six macular locations (L1-L6 in Fig. 1B): three above and three below the horizontal midline (HML) at 3°, 6° and 12° temporal retinal eccentricities. An additional 12° location (L7, between L5 and L6) was imaged at the temporal HML in one participant to examine the disease transition zone. The locations were designed to capture RGC regional differences from the HD. For each retinal location, 20–30 AO-OCT videos (10 volumes/video) were acquired over ~15 min. The volumes covered a 1.5° × 1.5° FOV with 300 A-scan/B-scan and 300 B-scan/C-scan to achieve a lateral pixel density of 1.5 µm/pixel in both axes. Fast A-scan, B-scan, and C-scan rates of 210 kHz, 700 Hz, and 2.3 Hz reduced, but did not eliminate, eye motion artifacts.

AO Image Analysis

AO-OCT volumes were reconstructed, dewarped to correct nonlinearities in the fast-axis scan direction, registered in three dimensions with sub-pixel accuracy using a custom algorithm[36,42] to correct eye motion artifacts, and averaged to increase the signal-to-noise ratio. The registered and averaged volumes were used for further morphological analyses. Retinal images were corrected for eye length and converted from degrees to millimeters according to the method introduced by Bennett et al.[43] We first manually marked GCL soma coordinates (x, y, z) using custom developed software in MATLAB (Mathworks Inc., Natick, MA, USA), which permits reliable cell identification through simultaneous visualization of B-scans in both fast and slow directions and an en face projection at the depth-of-interest (Supplementary Video S1). The software also allows switching between linear and logarithmic scaling for image display and adjusting intensity for optimal visualization to aid the cell counting process. The cell counts on every volume were verified by two experienced graders. The GCL somas coordinates were then used to compute soma density and diameter. Because we do not distinguish RGCs from displaced amacrine cells that are known to reside in this layer, throughout the article we use the term GCL soma rather than RGC, although the cells in this layer are predominantly RGCs (displaced amacrine cell percentage varies from 3% at 3° to 22% at 12°) according to histologic evidence.[44] To calculate GCL soma density, the GCL soma centers were projected onto a single en face plane and Voronoi mapping was applied to the soma mosaic, a mathematical construct widely used to quantify

Investigative Ophthalmology & Visual Science

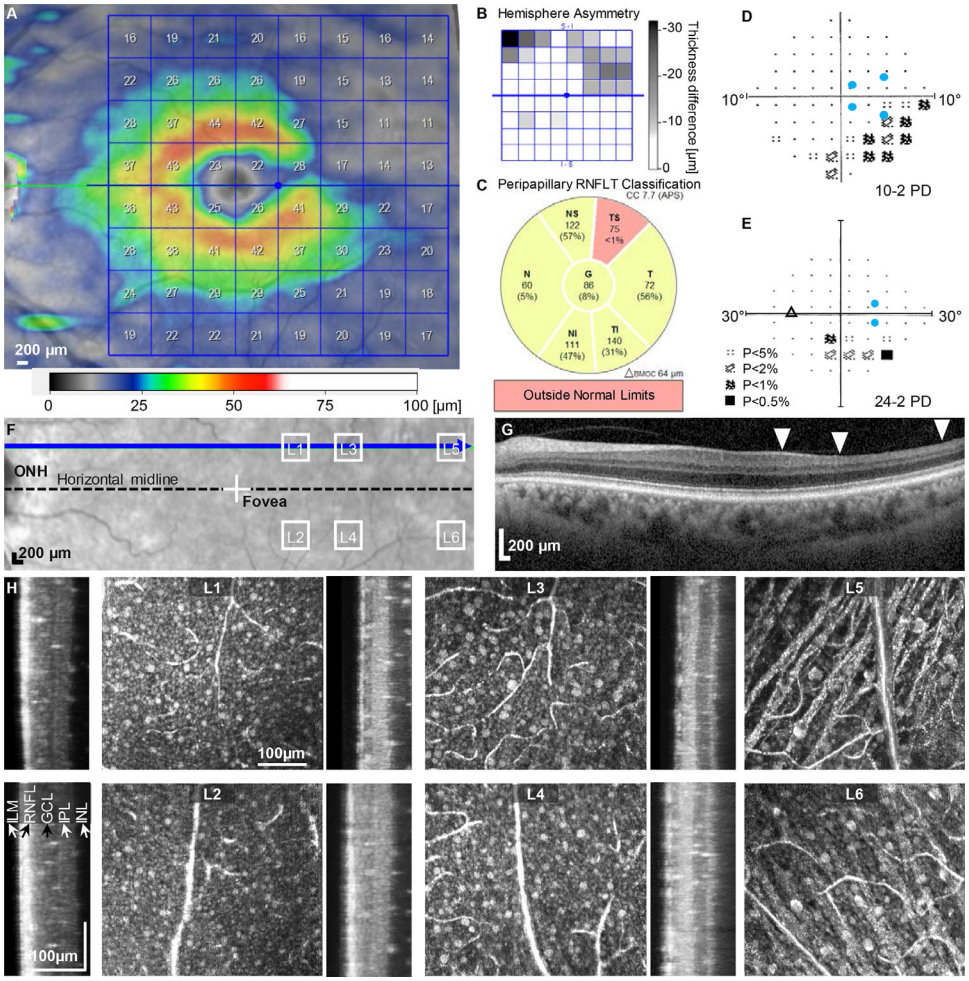

Figure 2. Images of the left eye of a 51-year-old glaucoma patient (1733) with superior hemifield defect. Clinical data include (**A**) optical coherence tomography (OCT) macula ganglion cell layer (GCL) thickness measurement, (**B**) hemisphere asymmetry map, (**C**) peripapillary retinal nerve fiber layer thickness classification, (**D**) 10-2, and (**E**) 24-2 VF PD maps, (**F**) Spectralis scanning laser ophthalmoscopy macula scan, and (**G**) OCT B-scan at 2.5° superior retina (denoted by *blue arrow line* in **F**). The *light blue dots* shown in the VF maps (**D** and **E**) correspond to the AO-OCT imaged locations at 3°, 6°, and 12°, respectively. OCT B-scan showed thinning of inner retina. The three *white arrowheads* associate with the three superior locations (*L1*, *L3*, and *L5*) in **F**. (**H**) AO-OCT B-scan and en face projection (single plane) at six retinal locations (*L1–L6*) showed a significant decrease in GCL soma density in the superior retina correlated with the HD. Representative three-dimensional volumetric visualization of 12°(L5) data set showed in Supplemental Video S2. B-scans at the paired locations were approximately aligned to the IPL for comparison. RNFL, retinal nerve fiber layer; optic nerve head (ONH), ILM, inner limiting membrane; RNFL, retinal nerve fiber layer; GCL, ganglion cell layer; IPL, inner plexiform layer; INL, inner nuclear layer.

retinal cells.[36] The GCL soma density was defined as the ratio of total number of Voronoi cells to the total area of the Voronoi cells. The proportion of normal GCL soma was calculated by normalizing to the averaged soma density from the control group at the corresponding location in both units of percentage (Density[glaucoma]/Density[control]) and dB (−10log [% of normal cells]) for easier comparison to VF measurements reported in dB units. We manually excluded areas that contained blood vessels for accurate density calculation. The diameter of each GCL soma was computed using an en face projection spanning three axial pixels (~2 µm) from the soma center. A radial profile from the soma center was generated and superimposed on the soma en face display to guide soma size measurement by defining a region of interest. The cell diameter was measured as twice the distance between the cell center and the minimum in the radial profile within the region of interest determined from the visualization. With measured GCL soma density, we examined regional differences in our subjects. Symmetry was defined as the density ratio between pairs of locations situated about the midline (Superior-Inferior [S-I]) at the same retinal eccentricity: Symmetry = Min(Density[S,I])/Max(Density[S,I]). By definition, symmetry ranges from 0 to 1 and thus is a simple metric to investigate regional HD severity in glaucoma.

Clinical Data Analysis

VF and OCT measurements qualified for the quality criteria.[45] VF measurements met the reliability criteria of the Humphrey visual field test (i.e., <20% fixation losses and <15% false-positive errors) and OCT images reached a quality standard of 20.[46] From each subject's clinical record, we extracted retinal thickness measurements from the clinical OCT scans (Supplementary material) and visual function maps from the Humphrey VF tests. Automatic OCT retinal

Investigative Ophthalmology & Visual Science

layer segmentation was confirmed and compared at the AO imaging locations, accounting for the raphe angle (Supplementary material). To determine the VF pattern deviation (PD) values in regions corresponding to AO imaged locations, VF 24-2 and VF 10-2 maps were used, accounting for the displacement in GC receptive fields with respect to the VF location.[47] The blue dots in Figures 2D and 2E indicate the location from which the PD values were extracted, interpolated from the lower sampled VF maps. We used VF 10-2 maps to calculate the PD values for 3° and 6° locations, and VF 24-2 maps for 12° locations. On one subject (7365), the VF 10-2 map was not available, therefore PD values at all locations were extracted solely from the VF 24-2 map. The OCT and VF measurements are summarized in Supplementary Tables S1 and S2 for the glaucoma and control cohorts, respectively. The GCL thickness in glaucoma subjects is normalized to that of the controls at corresponding locations calculated in both units of percentage (thickness[glaucoma]/thickness[control]) and dB (−10log[% of normal thickness]).

Statistical Methods

Glaucoma and control cohorts were compared on age, race, sex, axial length, CDR, IOP, OCT RNFL thickness, and VF metrics. Continuous variables were compared using an independent Student's *t*-test and categorical variables were compared using χ^2 analyses.

GCL soma density, soma diameter, and symmetry were compared at each retinal eccentricity (3°, 6°, and 12°) between glaucoma subjects and controls. GCL density and soma size in the paired retinal eccentricities (S-I, see Fig. 1B) were also compared in the glaucoma group to investigate their correspondence with HD. The comparisons were done using Student's *t*-test. Functional loss (PD) was compared with structural loss from both clinical OCT GCL measurements and AO-OCT GCL soma density using Deming regression model. The Deming regression model was also used to correlate AO-OCT GCL soma density with clinical OCT GCL thickness measurements. As individuals were age-matched, we did not adjust our analyses for age. Statistical analysis was done with SPSS (IBM, Armonk, NY, USA), Excel, and MATLAB (MathWorks, Inc., Natick, MA, USA).

Results

The Table shows demographic and ocular characteristics of the glaucoma patients and age-matched controls. There were no statistically significant differences between each group in terms of age, race, and axial length. The control group consisted of six male subjects. As expected, the CDR was significantly larger and the RNFL was significantly thinner in glaucoma patients than controls. IOP was being treated in the glaucoma subjects, and there was no significant difference in IOP between the two groups.

Table. Subject Demographic and Ocular Characteristics

	Glaucoma (n = 6)	Control (n = 6)
Age (years)	58.1 ± 4.5	61.1 ± 8.3
Race		
White	3 (50%)	5 (83.3%)
Non-white	3 (50%)	1 (16.7%)
Sex*		
Male	1 (16.7%)	6 (100%)
Female	5 (83.3%)	0 (0%)
Axial Length (mm)	23.8 ± 1.2	24.4 ± 1.4
CDR*	0.6 ± 0.2	0.4 ± 0.1
IOP (mm Hg)	13.5 ± 2.6	16.5 ± 4.2
RNFL (overall)* (um)	79.3 ± 11.3	92.7 ± 6.5
VFI 24-2 (%)	91 ± 0.06	
MD 24-2 (dB)	−2.7 ± 2.8	
PSD 24-2 (dB)	3.7 ± 1.1	
MD 10-2 (dB)	−4.1 ± 2.6	
PSD 10-2 (dB)	5.2 +/− 4.2	

CDR, cup-to-disc ratio; IOP, intraocular pressure; RNFL, retinal nerve fiber layer; VFI, visual field index; MD, mean deviation; PSD, pattern standard deviation.
* $P < 0.05$.

AO-OCT Quantification of GCL Soma Morphology

GCL soma mosaics were successfully resolved in the recorded volumes at different retinal locations in subjects from both cohorts (Supplemental Video S1). As expected, in the healthy control cohort, GCL thickness decreased from 4-5 cell layers at 3° (L1 and L2) to 2-3 cell layers at 6° (L3 and L4) and further reduced to a monolayer at 12° (L5 and L6, B-scan images in Fig. 1D). This corresponds to a GCL soma density (average between the two locations at the same temporal eccentricity) of 29,304 cells/mm^2 at 3°, 13,656 cells/mm^2 at 6°, and 4582 cells/mm^2 at 12° for the subject shown in Figure 1. GCL somas are small and homogeneous in size at lower retinal eccentricities (en face images in Fig. 1D at L1 and L2) and larger and more variable at higher retinal eccentricities (en face images in Fig. 1D at L5 and L6).

In contrast, these morphological parameters are more variable and noticeably different in the glaucoma cohort. For example, in a 51-year-old patient with early glaucoma (Fig. 2) whose deficits occurred at the superior-temporal retina (Figs. 2B, 2C), a reduction of GCL thickness and soma density was observed throughout all examined retinal locations but more predominantly in the superior hemifield locations (B-scan images from L1, L3, and L5 in Fig. 2H). The PD was −1.9 dB, −2.4 dB, and −2.3 dB in the corresponding inferior patches from the VF maps (superior retinal patches; Figs. 2D, 2E), indicating a correspondence between GCL soma loss and vision loss in glaucoma. When compared with the relatively healthier hemifields at the higher eccentricities (L3–L6), the clinical VF measurement showed the superior retinal patches (inferior VF patches; mean = −2.4 dB) have 1.4 dB more function loss compared to the inferior retinal patches (mean = −1.0 dB), while the superior retina (−4.86 dB) had 4.15 dB more loss in GCL soma density than the inferior retina (−0.71 dB). Similarly, clinical OCT GCL thickness measurements (Figs. 2A, 2G) showed −0.34 dB and −2.50 dB loss at inferior and superior retinal locations, respectively (Supplementary Table S1). Interestingly, the clinical measurements of VF indicated the 6° superior patch was damaged the most by glaucoma (−2.5 dB at L3; −2.31 dB at L5), whereas the structural measurement of clinical OCT (−2.40 dB at L3; −2.59 dB at L5) showed most injury occurred at 12° consistent with our AO-OCT data (−3.84 dB at L3; −5.87 dB at L5). We observed a gradual increase in soma size with eccentricity in the glaucoma subject (Fig. 2H) similar to that found in the control subject (Fig. 1D). In contrast to the control subject results, significantly enlarged cells were observed, which was more

Investigative Ophthalmology & Visual Science

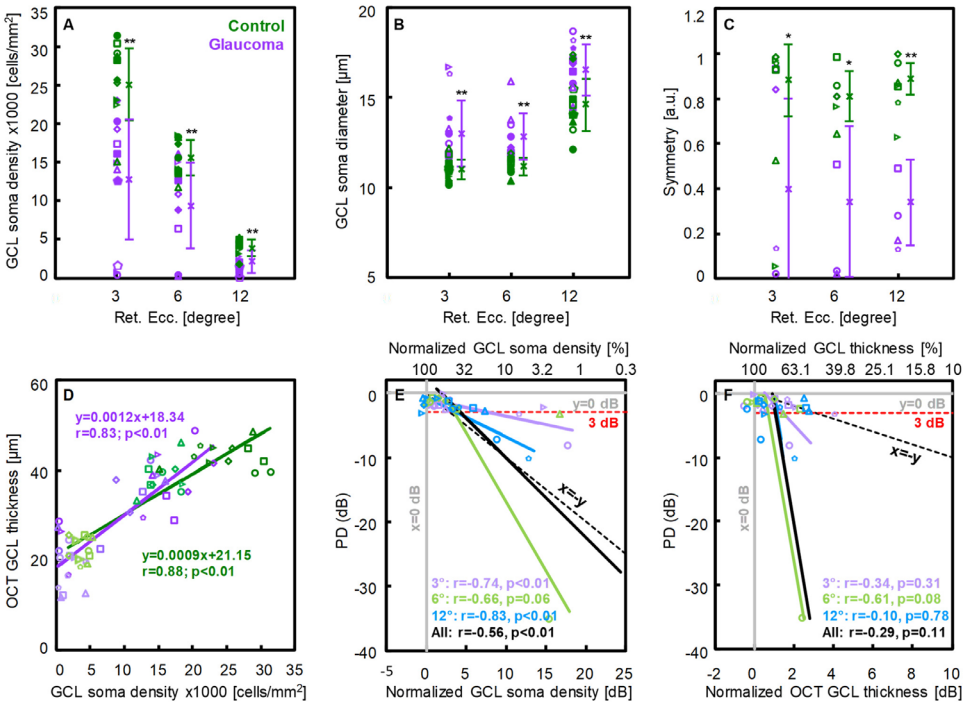

Figure 3. AO-OCT quantification of (**A**) ganglion cell layer (GCL) soma density, (**B**) Soma diameter, (**C**) Symmetry, and correlations between (**D**) Adaptive optics–optical coherence tomography (AO-OCT) measured GCL soma density and OCT (Spectralis) measured GCL thickness, (**E**) Adaptive optics–optical coherence tomography (AO-OCT) measured GCL soma density percentage and pattern deviation (PD), and (**F**) clinical OCT measured GCL thickness percentage and PD. A statistically significant difference was revealed between the glaucoma (*purple*) and control (*green*) groups in terms of GCL soma density, diameter and symmetry. Glaucoma caused cell morphology changes correlated with the hemifield defect. Open purple symbols (○) in (A) and (B) denote more diseased hemifield and filled purple symbols (●) represent relatively healthier hemifield. For the control group, open green symbols were from (○) superior retina and filled green symbols (●) are from inferior retina. In each plot, different symbols represent different subjects. In (D) data is color-coded with respect to eccentricity: 3° data in darkest color symbol and 12° in lightest color symbol. Colors in (E) and (F) are coded with respect to retinal eccentricities, and the percentage was normalized to control eyes. The black dashed line denotes x = −y that indicates an equal rate of structural and functional loss. While the true structure-function relationship is non-linear and more complex, a coarse rule-of-thumb is that datapoints above the x = −y line (log-log scaling) represent structural losses preceding functional loss and datapoints below represent the opposite.[18] The red dashed line denotes 3 dB PD loss. *P*-Value < 0.01 **, and *P*-Value < 0.05 * (Students' t-test). r in (D-E) is the Pearson correlation coefficient.

pronounced in the peripheral locations at 12° and correlated with the orientation of the HD.

The morphological parameters were quantified in both cohorts (Fig. 3, Supplementary Fig. S1). Consistent with our visual assessment in Fig. 1 and Fig. 2, GCL soma density is significantly lower in the glaucoma group (purple symbols in Fig. 3A) than the age-matched healthy controls (green symbols in Fig. 3A) regardless of retinal eccentricity. GCL soma density peaked at 3° (mean ± SD = 25,058 ± 4649 cells/mm^2), decreased at 6° (15,551 ± 2301 cells/mm^2), and further reduced at 12° (3891 ± 1105 cells/mm^2) in the control group. In contrast, the GCL soma density in the glaucoma group was lower in all eccentricities with values of 12,799 ± 7747 cells/mm^2, 9370 ± 5572 cells/mm^2, and 2134 ± 1494 cells/mm^2 at 3°, 6°, and 12°, respectively, representing a 49%, 40%, and 45% decrease in glaucoma subjects as compared to control subjects. The soma density is highly correlated with clinical GCL thickness in the control group (green line in Fig. 3D) with $r = 0.88$, and somewhat less correlated ($r = 0.83$) in the glaucoma group (purple line in Fig. 3D). This suggests that GCL thickness may be a degraded surrogate with which to estimate GCL soma density in early to moderate glaucoma. Interestingly, we also found that the density reduction (i.e., symmetry change, Fig. 3C) was approximately the same for all eccentricities, suggesting the disease causes cell loss more equally across the macula than previously thought, though intrasubject differences remain. Symmetry appears to be a robust metric and potential predictor for glaucoma that manifest with hemifield defects, as the vast majority of control subject's values ranged from 0.75 to 1.0 whereas every glaucoma subject had at least one location well outside of that range.

As we observed visually, GCL soma size was significantly larger in glaucoma patients at all eccentricities. Like the control group, GCL soma diameter in the glaucoma group was largest at 12° (mean ± SD = 16.5 ± 1.4 μm) and smaller at 6° (12.8 ± 1.3 μm) and 3° (13.0 ± 1.8 μm), but significantly larger than the control group (12°: 14.6 ± 1.5 μm; 6°: 11.6 ± 0.5 μm; 3°:11.0 ± 0.6 μm, with $P < 0.01$ at all locations), representing an increase of 18%, 15%, and 13%.

The structural measurements of AO-OCT GCL soma density (Fig. 3E) and clinical OCT GCL thickness (Fig. 3F) both correlate with functional VF PD measurements, but the correlation with AO-OCT–measured density was significantly stronger (r range: −0.66 to −0.83 with $P < 0.01$ at 3° and 12° and $P = 0.06$ at 6°) than clinical OCT measured thickness (r range: −0.10 to 0.61). The slightly increased P value at 6° in Figure 3E is likely caused by the extremely large PD value (−35 dB) from one subject

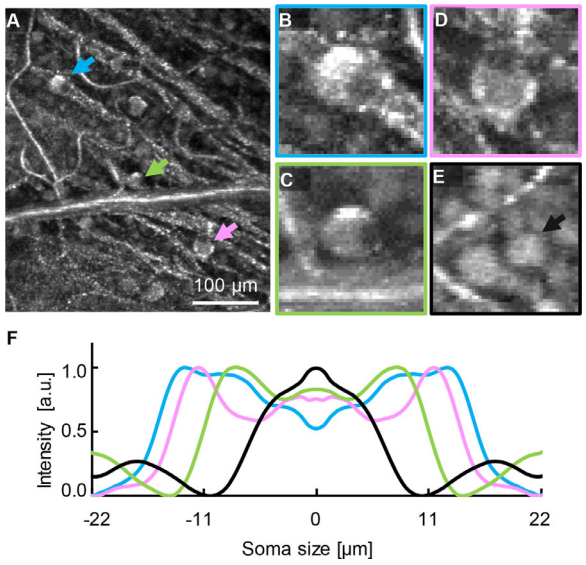

Figure 4. AO-OCT revealed subcellular reflectance changes in ganglion cell layer (GCL) somas in a 51-year-old early glaucoma patient (1733) at 12° (L5). (**A**) Representative AO-OCT en face image showed reflectance variations of three identified cells (*arrows*). (**B–D**) Magnified regions (65 µm × 65 µm) of the cells labeled in (**A**). (**E**) Magnified region of GCL somas from the same eccentricity of a 49-year-old healthy subject. (**F**) Radial profiles from the center of the cell reveal a distinctive pattern associated with subcellular hyporeflectivity in comparison to normal function in control subjects.

(green filled circle), which consequently resulted in a slope larger than one ($x = -y$) for the Deming regression curve (green line). Regardless of the locational difference, the data showed high correlation between PD and GCL soma density (black line).

GCL Soma Reflectance Changes With Glaucoma

Besides morphological differences, we also observed subcellular reflectance changes in GCL somas from glaucomatous eyes. In three out of six glaucoma eyes, subcellular changes were observed in the enlarged RGC somas (up to 38 µm) including a ~15 µm diameter eccentric hyporeflective region thought to be the cell nucleus (Figs. 4B, 4C). In addition to a hyporeflective nuclear region, another of the cells (Fig. 4D) also shows a cytoplasm that reflects less light than the surrounding cell wall. In comparison, no cells with similar appearance were observed in the control eyes, and the reflectance of healthy cells had a uniform intensity distribution across the cell bodies (Figs. 4E, 4F) with much smaller soma size (Fig. 4E). Similar results (heterogeneous cellular reflectance) were also observed in another two moderate glaucoma patients (see Supplemental Figs. S2 and S3). This optical signature indicates a change in subcellular composition and may serve as potential biomarker of RGC health. Further evidence and follow-up imaging are required to verify this hypothesis.

In addition, AO-OCT revealed hyperreflective clustered structures in the IPL (Fig. 5 and Supplementary Fig. S3 and Supplementary Video S3 frames 43–58) in two subjects. In contrast, the IPL en face projection in healthy eyes showed no similar hyperreflective clustered structures (through 3D volumetric visualization of AO-OCT volumes) at any location (of 36 total examined retinal locations) but exhibited as a homogenous field with fully developed speckle patterns in the OCT volumes (Supplementary Fig. S3). The hyperreflective clustered structures were located only on the HD side and only at lower eccentricities − 3° and 6° but not 12°. Axially, the structures were predominantly located in the anterior (inner) portion of the IPL (Fig. 5C and Supplementary Video S3). The hyperreflective structures were 9 µm to 15 µm in diameter and distributed across the entire 1.5° field. Compared to GCL somas, the IPL structures are brighter, suggesting a large refractive index mismatch to the surrounding GCL dendritic fields. A hyporeflective region (Supplemental Video S3 frames 106–130) was also observed in the inner nuclear layer at the L2 location, which is likely a microcytic lesion.[32]

Tracking Inner Retinal Changes

With high resolution volumetric imaging and subcellular accuracy registration, our AO-OCT method not only allows study of morphological changes caused by pathology but also offers a powerful tool to monitor disease progression or assess the efficacy of surgical intervention. One patient with early glaucoma, elevated IOP (25–30 mm Hg), and retinal thinning in one hemifield enrolled in our study and underwent AO-OCT imaging. The patient's IOP subsequently could not be controlled with medication and Kahook dual blade goniotomy, resulting in further glaucomatous progression with worsening of VF and progression to moderate glaucoma. The patient then underwent combined phacoemulsification and trabeculectomy with mitomycin C. One month after trabeculectomy (approximately eight months after initial imaging session), the patient's IOP was 6 to 7 mm Hg, and the patient underwent repeat imaging with AO-OCT. There was a noticeable visual field loss found between the two visits (VF 24-2: MD change from −2.72 dB to −7.75 dB and pattern standard deviation from 2.24 dB to 6.06 dB). At the time of imaging, no evidence of postoperative macular edema was found by OCT examination. The inner retinal structural changes between visits were compared in Figure 6. Although the visits were only eight months apart, significant soma reduction was evident in both AO-OCT B-scan (Figs. 6A, 6B) and en face projections (Figs. 6C, 6D), resulting in GCL density decrease from 14,098 cells/mm^2 to 3791 cells/mm^2 at location L2, 16,039 cells/mm^2 to 10,260 cells/mm^2 at L3, 4250 cells/mm^2 to 1506 cells/mm^2 at location L5, and 720 cells/mm^2 to 329 cells/mm^2 at location L6 (Supplementary Figs. S4 and S5). This represented a decrease of 73%, 36%, 54%, and 64%, suggesting that the patient experienced the greatest ganglion cell loss at lower retinal eccentricity. The magnified regions shown in Figure. 6E detailed GCL soma loss (white arrows) at the time of the second visit. In addition, there are regions where the cells are obviously enlarged, indicating not just that the smaller cells died, though this may have occurred as well (Supplementary Fig. S5). The significant collapse of the GCL parenchyma resulted in vascular plexus displacement and compression in depth (Figs. 6G, 6H). For example, the labeled branching vessels (arrows) have migrated from the anterior (red) to the posterior (green) part of the GCL. The extensive GCL tissue remodeling is associated with IPL thinning in the defective hemifield (Supplemental Table S1) during the dynamic disease progression (Fig. 6F). Similar results were found at additional three locations from the same patient (Supplementary Fig. S5). Future

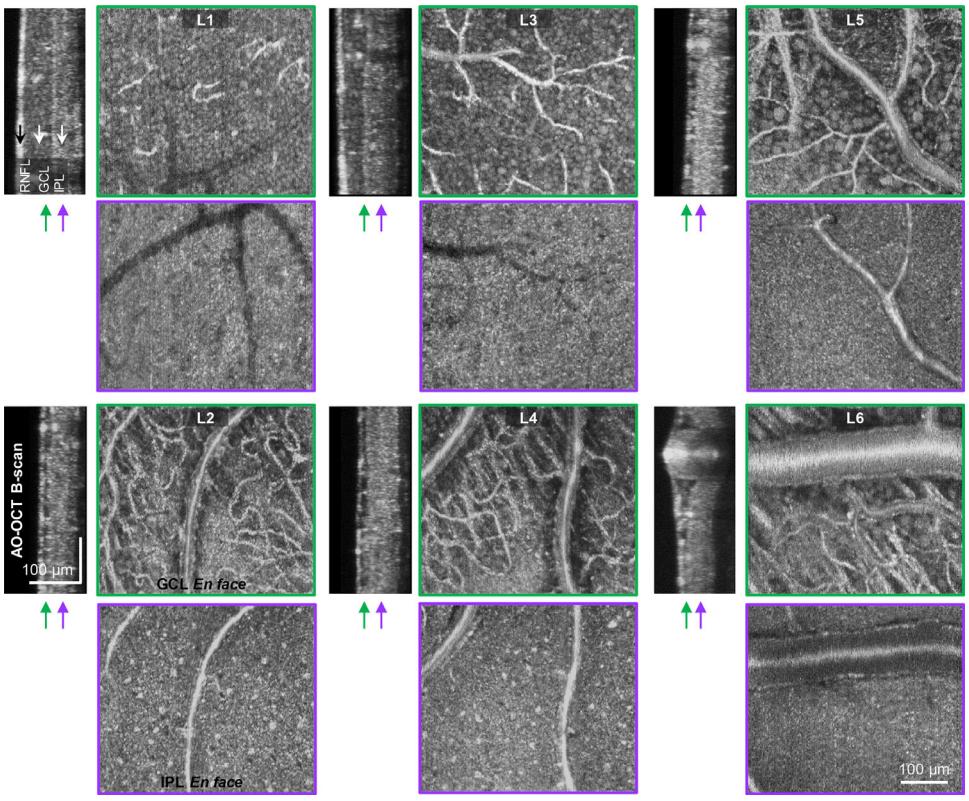

Figure 5. AO-OCT reveals hyperreflective structures in the defective hemifield (inferior retina) in the right eye of a 62-year-old glaucoma patient (1541, also see Supplemental Video S3 for the three-dimensional volumetric visualization of Adaptive optics–optical coherence tomography (AO-OCT) data taken at L2). Adaptive optics–optical coherence tomography (AO-OCT) B-scan and en face projections at six retinal locations (L1–L6) show a significant soma density reduction in the ganglion cell layer (GCL) (green) in the inferior retina correlated with the HD. hyperreflective structures were seen from en face projections of the inner plexiform layer (IPL) (purple) in two inferior retinal locations (L2 and L4). B-scans at the paired locations were approximately aligned to the IPL for comparison purpose. RNFL, retinal nerve fiber layer.

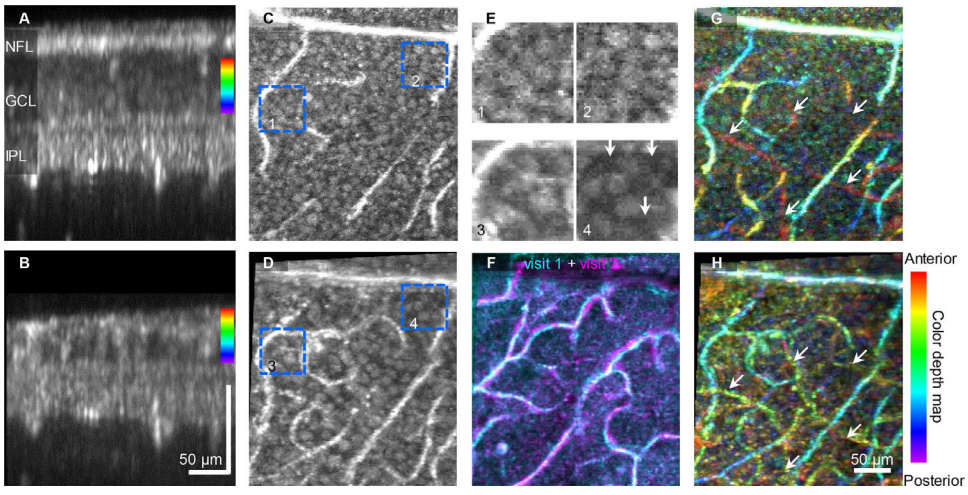

Figure 6. AO-OCT tracking of inner retinal changes at a 3° retinal location (L2) in the right eye of a 58-year-old patient (7365) with two visits. B-scan images taken: (**A**) first visit and (**B**) second visit. The Adaptive optics–optical coherence tomography (AO-OCT) volumes between the two visits were axially aligned to the top of IPL for comparison purpose. En face projection across 10 pixels (~7 µm) of the ganglion cell layer (GCL) soma mosaic taken at (**C**) first visit and (**D**) second visit. (**E**) Magnified views of two labeled regions (*blue boxes*) from two visits. (**F**) Color merged en face projection across 20 pixels (~14 µm) of IPL vessels between first (cyan) and second (magenta) visits demonstrated good registration and little vascular remodeling. Depth color maps showed superficial vessels in GCL in first visit (G) migrated posteriorly in the second visit in (H). The example branching vessel is labeled with *white arrows*. IPL, inner plexiform layer; NFL, nerve fiber layer.

Investigative Ophthalmology & Visual Science

AO imaging sessions will assess other aspects of glaucoma progression and surgical outcomes.

Discussion

We present, for the first time, an in vivo investigation of GCL morphology changes in POAG patients using high-resolution AO-OCT. The main findings of this study and comparison with age-matched controls, as well as with current understanding of glaucoma are highlighted below.

GCL Soma Density and Size Change in Glaucoma

GCL soma density was significantly lower and soma size was significantly greater in the glaucoma cohort compared to the control group (Figs. 1–3), where control subject results were consistent with previous in vivo human measurements[35,36] and histology studies[44,48–51] (Supplementary Fig. S6). The lower GCL soma density and greater soma diameter corresponded to subjects' hemifield defects, which reflects glaucoma related effects rather than imaging artifacts (Supplemental material).

Given the fact that clinical OCT has long established the loss of RNFL and GCL layer thickness with glaucoma, the observation that GCL soma density decreased in early and moderate glaucoma was not an unexpected result. How soma size changes in glaucoma has been long debated. The effect of glaucoma on RGC body size during cell death has been studied by a variety of techniques, and in both human postmortem tissue and animal models. A number of reports suggest that, although all RGC types are ultimately susceptible to glaucoma, larger cells like parasol RGCs (pRGC) with larger axon diameters die preferentially in human glaucoma and in experimental glaucoma animal models.[3,11–13] These results do not seem to agree with our findings. By visual assessment, the ratio of large pRGC to smaller midget RGCs (mRGC) appears higher in glaucoma eyes (Fig. 2F) than in heathy controls (Fig. 1D). This is further substantiated by the AO images collected from a glaucomatous eye across the transition zone (Supplementary Fig. S2), which show no evidence of selective parasol cell death. In fact, our results are in line with a psychophysical study that was supportive of neural adaptation abnormalities in early glaucoma.[52] The discrepancy may be the result of differences between glaucoma in humans and animal models or due to the disease severity stage. In animal models, glaucoma is induced with an acute IOP increase that may substantially differ from human glaucoma inception, particularly with respect to non-IOP related factors. Previous studies in glaucoma animal models also show evidence of increased RGC soma area,[14–16] and soma enlargement has been suggested to be compensatory to cell loss. Our results from six early- to moderate-stage glaucomatous eyes support the view that the spaces vacated after phagocytosis may induce the remaining RGCs to increase size. Although in this study we did not quantitatively differentiate among RGC types (GCL is primarily occupied by mRGCs and pRGCs, and the displaced Amacrine cells are about the size of mRGCs[44]) and displaced Amacrine cells, we did observe a gradient in soma size and some separation in their histogram (not shown) that suggests the surviving GCL somas are likely a combination of all three types. In disease conditions with cell body enlargement, cell classification is even more challenging because it requires a priori knowledge of enlarged cell type, which could presumably be gathered by tracking the cells over time across stages of disease development with verification of reproducibility. There is some evidence that the change in RGC soma size may also depend upon disease severity,[15] cup-to-disc ratio,[11] retinal eccentricity,[11] and RGC cell types[12]; however, these factors are outside of the scope of this study. A comprehensive picture of all mechanisms that lead to an increase in GCL soma diameter with glaucoma is an on-going effort, and our results help provide a foundation for further study. Nevertheless, perhaps one possible explanation for the cause of soma enlargement could be structural damage in the RGC cell body (e.g., cell fragmentation during apoptosis) causing transformation of soma shape from spherical to flatter, disc-shaped in the axial dimension. This conclusion is supported by our data at 12 degrees (Fig. 2H, Fig. 5, and Supplementary Fig. S2), where the somas formed a monolayer, and cell enlargement is evident in the en face plane accompanied by a reduction of cell height (layer thinning) in the axial dimension. Regardless of the disease caused layer thinning, somas remain mainly spherically-shaped as measured in the en face plane (Supplementary Fig. S7). Because our soma diameter measurement method is extracted in the en face plane around the cell center, cell enlargement is readily gleaned from our analysis. However, other morphological parameters, particularly those that take advantage of AO-OCT's inherent micron-resolution volumetric capabilities, such as soma height, soma volume, or height-to-width ratio may also help describe RGC health. This soon could become feasible with an approach that masks the RGC soma in 3D.[53]

Regional Effects of Glaucoma

While glaucomatous damage had historically been thought to proceed from the periphery inward, recent studies indicate that the central macula may be as affected as the peripheral retina both structurally and functionally.[6] Clinical OCT has indicated glaucoma damage can be widespread as well as local, and OCT macula scans are widely used for glaucoma detection.[6] Furthermore, it has long been understood that the arcuate nerve fiber bundles can be differentially affected by glaucoma according to the location they enter the optic nerve head. Our study design sought to reveal regional cellular morphological changes in glaucoma, both central and peripheral, but also with respect to field effects like hemifield defects. Our results indicate that RGCs are affected equally across the macula by glaucoma, although RGC loss affects vision proportionally more in the periphery, probably owing to reduced RGC density, cone-to-RGC ratio, and lower redundancy in peripheral regions. Unsurprisingly, we also observed that GCL cell loss corresponded to all prior clinical evidence of each subject's HD.

Structural and Functional Correlation in Glaucomatous Eyes

For reasons to do with the promise of new early therapies, another question that has been debated is "Does structural damage precede visual function loss in glaucoma?"[18] Our ability to resolve individual GCL somas allows correlation of structural soma loss with functional vision loss. We compared AO-OCT density measurements with functional VF tests (Fig. 3 E), and found that the regions with largest

Investigative Ophthalmology & Visual Science

percentage of cell loss did not necessarily correspond to those with the most functional impairment. This could be explained by the functional implications imposed by mRGC sampling, where the normal mRGC/cone ratio decreases from 1.8 at 3° to 0.3 at 12°.[54] Thus the same proportion of cell loss in the periphery had greater consequences for vision than at 3°, as evident by the shallower slope at 3° (purple line). Similar to findings in diseases with photoreceptor loss[55] this indicates the redundancy and higher-order cortical processing, particularly with respect to central vision. We also found that considerable GCL soma loss does not result in significant functional loss, that is, in most subjects as much as 70% (~30% [5 dB] normal) of GCL soma were lost before 3 dB functional loss was detected in VF testing (Fig. 3E). When more than 70% of GCL somas are lost, vision degrades rapidly and more variably. Our results imply that in early-stage glaucoma measured in this study, structural losses exceeded the functional losses, and the structural-functional correlation may be location dependent. Applying similar analysis to the clinical OCT GCL thickness measurements, we found a greater percentage of datapoints below the x = −y line (Fig. 3F), supporting perhaps the opposite conclusion that functional losses may precede structural losses.[56] This observation is likely a consequences of the "floor effect" that diminishes the significance of thickness measurements in moderate to severe glaucomatous eyes, despite the evidence that OCT diagnosis is preferred to functional VF testing in early disease development.[5] Intriguingly, in the example of a moderate glaucoma patient (Supplementary Fig. S2), our method captured increased GCL soma loss across the transition zone (L5: 1501 cells/mm^2, L7 = 447 cells/mm^2, and L6 = 198 cells/mm^2), whereas clinical OCT exhibited only a minor change in GCL thickness (L5: 17.8 µm, L7 = 23.2 µm, and L6 = 18.2 µm). All of the above results suggest that cellular-level GCL soma detection is a more sensitive metric to track structural losses compared to clinical OCT GCL thickness measurements. The results from our relatively small study, particularly with respect to the structure-function relationship and detection sensitivity, should be confirmed with a larger clinical study, including longitudinal tracking of soma changes across all disease stages. Nevertheless, our study is one of the first to explore these issues on the cellular level in early to moderate glaucoma.

Other Associated Cellular Change and Sensitive AO Biomarkers for Glaucoma

Besides the morphological characteristics (density, soma size, and asymmetry) discussed above, AO-OCT also revealed other cellular features that are associated with glaucoma, and those unique optical characteristics presumably could be potential sensitive biomarkers for glaucoma. One salient feature we observed was the altered reflectance of GCL somas in glaucomatous eyes. The observed reflectance variation likely occurred in the RGC cells rather than other cells in the GCL, such as macrophages, which have different morphological and optical characteristics and showed unique spatial and temporal features compared to those observed in Figure 4.[23,36,57–59] Large hyporeflective regions that may indicate clumping of chromatin in the nuclei in the cytoplasm of the cell (Figs. 4B, 4C) are a feature of apoptosis seen in histology,[3,60] and the reflectance variance (Fig. 4D) may suggest that the dead cell has been engulfed by a neighboring cell. Apoptosis in glaucoma patients has been detected using SLO and an intravenously administered fluorescent marker.[61] AO-OCT may provide a label-free method for apoptosis detection. Validation of reflectance changes with apoptosis will require tracking cells over time, which has been proven technically feasible in this study (Fig. 6 and Supplementary Fig. S5).

Another feature of the glaucomatous eye revealed by this study is the hyperreflective IPL structures which may be the result of tissue re-modeling in that layer. The IPL contains dendritic connections between RGCs and bipolar and amacrine cells,[62] as well as glial cells: microglia[63] and the stalks of Müller cells that span nearly the entire retina.[64,65] During glaucoma progression, the extensive RGC dendritic tree is pruned and retracts,[66–69] and this could possibly create denser structures that manifest as hyperreflectivity in OCT volumes. The axial location of the hyperreflective structures in the anterior portion of the layer probably rules out any association with horizontal cells and makes less likely any association with bipolar cells. Amacrine cells are known to be displaced as far as the GCL layer.[70] There appears to be no evidence of RGC migration into the IPL, even with disease. Whether the hyperreflective structures are activated microglia, displaced amacrine or ganglion cells, associated with RGC dendritic retraction, or an entirely other structure requires further investigation.

Altogether, the metrics described in the present study can be used as sensitive cellular biomarkers of RGC health and, with further study, enhance our understanding of glaucoma pathogenesis. In addition, the ability to accurately monitor RGC health longitudinally confers numerous benefits. First, our understanding of the natural history of glaucoma would be enhanced, perhaps highlighting spatial patterns of retinal cell death over days, weeks, and years. Second, AO-based cellular biomarkers could serve as tools to reliably measure the neuroprotective efficacy of therapeutic agents.[71] Last but not least, AO-OCT allows in vivo investigation of the interplay between different retinal cells, including immune cells.[59–72] In particular, retinal microglia are implicated in the development of many ocular and neurological diseases and may also provide potential treatment targets.[73] AO-OCT promises improved detection of glaucoma initiation and better insight into progression that will lead to better targeted treatment options to prevent visual damage and blindness.

Limitations

This pilot study has certain limitations inherent to its cross-sectional design and small sample size, potentially limiting generalizability. Although there was a significant difference in the sex of glaucoma and control subjects in our study, there is no consensus of a gender predilection in glaucoma. Our study looked at individuals with HD to compare regional GCL soma morphological characteristics in early to moderate disease development, but future studies should also incorporate suspect subjects, as well as those with advanced glaucoma and preperimetric glaucoma. Larger prospective studies will improve on the current work. AO allows for cellular and subcellular levels of resolution, with the tradeoff that the FOV are relatively small. This means that areas with abnormal GCL soma morphology may not reflect conditions across larger macular areas and local damage may not be captured by our chosen imaging locations. The number of imaging locations is

fundamentally limited by the significant averaging required to resolve GCL somas,[36] but with further increases in OCT acquisition speed,[74] a suitably time-bound clinical protocol can be developed.

Acknowledgments

The authors thank Donald Miller (Indiana University School of Optometry) for use of OCT 3-D registration software.

Supported by a grant from the FDA Critical Path Initiative and the intramural research program of the National Institutes of Health, National Eye Institute and an NIH Career Development Award (K23EY025014) (O.S.).

Initial results of this study have been submitted for presentation in the following conference meetings: ARVO 2019, SPIE Photonics West 2020, and ARVO 2020.

Disclosure: **Z. Liu,** adaptive optics–optical coherence tomography technology (P); **O. Saeedi,** Heidelberg Engineering (F); **F. Zhang,** adaptive optics–optical coherence tomography technology (P); **R. Villanueva,** None; **S. Asanad,** None; **A. Agrawal,** None; **D.X. Hammer,** None

References

1. Tham YC, Li X, Wong TY, Quigley HA, Aung T, Cheng CY. Global prevalence of glaucoma and projections of glaucoma burden through 2040: a systematic review and meta-analysis. *Ophthalmology*. 2014;121:2081–2090.
2. Nickells RW. From ocular hypertension to ganglion cell death: a theoretical sequence of events leading to glaucoma. *Can J Ophthalmol*. 2007;42:278–287.
3. Quigley HA. Neuronal death in glaucoma. *Prog Retin Eye Res*. 1999;18:39–57.
4. Saeedi OJ, Elze T, D'Acunto L, et al. Agreement and predictors of discordance of 6 visual field progression algorithms. *Ophthalmology*. 2019;126:822–828.
5. Zhang X, Dastiridou A, Francis BA, et al. Comparison of glaucoma progression detection by optical coherence tomography and visual field. *Am J Ophthalmol*. 2017;184:63–74.
6. Hood DC. Improving our understanding, and detection, of glaucomatous damage: An approach based upon optical coherence tomography (OCT). *Prog Retin Eye Res*. 2017;57:46–75.
7. Medeiros FA, Zangwill LM, Bowd C, Mansouri K, Weinreb RN. The structure and function relationship in glaucoma: implications for detection of progression and measurement of rates of change. *Invest Ophthalmol Vis Sci*. 2012;53:6939–6946.
8. Adams CM, Stacy R, Rangaswamy N, Bigelow C, Grosskreutz CL, Prasanna G. Glaucoma—next generation therapeutics: impossible to possible. *Pharm Res*. 2018;36(2):25.
9. Kuehn MH, Fingert JH, Kwon YH. Retinal ganglion cell death in glaucoma: mechanisms and neuroprotective strategies. *Ophthalmol Clin North Am*. 2005;18:383–395.
10. Liu Y, Pang IH. Challenges in the development of glaucoma neuroprotection therapy. *Cell Tissue Res*. 2013;353:253–260.
11. Weber AJ, Kaufman PL, Hubbard WC. Morphology of single ganglion cells in the glaucomatous primate retina. *Invest Ophthalmol Vis Sci*. 1998;39:2304–2320.
12. Morgan JE. Retinal ganglion cell shrinkage in glaucoma. *J Glaucoma*. 2002;11:365–370.
13. Glovinsky Y, Quigley HA, Dunkelberger GR. Retinal ganglion cell loss is size dependent in experimental glaucoma. *Invest Ophthalmol Vis Sci*. 1991;32:584–491.
14. Ahmed FA, Chaudhary P, Sharma SC. Effects of increased intraocular pressure on rat retinal ganglion cells. *Int J Dev Neurosci*. 2001;19:209–218.
15. Kalesnykas G, Oglesby EN, Zack DJ, et al. Retinal ganglion cell morphology after optic nerve crush and experimental glaucoma. *Invest Ophthalmol Vis Sci*. 2012;53:3847–3857.
16. Pinar-Sueiro S, Urcola H, Rivas MA, Vecino E. Prevention of retinal ganglion cell swelling by systemic brimonidine in a rat experimental glaucoma model. *Clin Exp Ophthalmol*. 2011;39:799–807.
17. Tribble JR, Vasalauskaite A, Redmond T, et al . Midget retinal ganglion cell dendritic and mitochondrial degeneration is an early feature of human glaucoma. *Brain Commun*. 2019;1(1):fcz035.
18. Hood DC. Does retinal ganglion cell loss precede visual field loss in glaucoma? *J Glaucoma*. 2019;28:945–951.
19. Williams DR. Imaging single cells in the living retina. *Vis Res*. 2011;51:1379–1396.
20. Jonnal RS, Kocaoglu OP, Zawadzki RJ, Liu Z, Miller DT, Werner JS. A review of adaptive optics optical coherence tomography: technical advances, scientific applications, and the future. *Invest Ophthalmol Vis Sci*. 2016;57(9):OCT51–OCT68.
21. Pircher M, Zawadzki RJ. Review of adaptive optics OCT (AO-OCT): principles and applications for retinal imaging [Invited]. *Biomed Opt Express*. 2017;8:2536–2562.
22. Burns SA, Elsner AE, Sapoznik KA, Warner RL, Gast TJ. Adaptive optics imaging of the human retina. *Prog Retin Eye Res*. 2018;68:1–30.
23. Miller DT, Kurokawa K. Cellular scale imaging of transparent retinal structures and processes using adaptive optics optical coherence tomography. *Annu Rev Vis Sci*. 2020;6:115–148.
24. Nadler Z, Wang B, Wollstein G, et al. Repeatability of in vivo 3D lamina cribrosa microarchitecture using adaptive optics spectral domain optical coherence tomography. *Biomed Opt Express*. 2014;5:1114–1123.
25. Akagi T, Hangai M, Takayama K, Nonaka A, Ooto S, Yoshimura N. In vivo imaging of lamina cribrosa pores by adaptive optics scanning laser ophthalmoscopy. *Invest Ophthalmol Vis Sci*. 2012;53:4111–4119.
26. Hood DC, Lee D, Jarukasetphon R, et al. Progression of local glaucomatous damage near fixation as seen with adaptive optics imaging. *Transl Vis Sci Technol*. 2017;6(4):6.
27. Takayama K, Ooto S, Hangai M, et al. High-resolution imaging of retinal nerve fiber bundles in glaucoma using adaptive optics scanning laser ophthalmoscopy. *Am J Ophthalmol*. 2013;155:870–881.
28. Chen MF, Chui TY, Alhadeff P, et al. Adaptive optics imaging of healthy and abnormal regions of retinal nerve fiber bundles of patients with glaucoma. *Invest Ophthalmol Vis Sci*. 2015;56:674–681.
29. Huang G, Luo T, Gast TJ, Burns SA, Malinovsky VE, Swanson WH. Imaging glaucomatous damage across the temporal raphe. *Invest Ophthalmol Vis Sci*. 2015;56:3496–3504.
30. Swanson WH, King BJ, Burns SA. Within-subject variability in human retinal nerve fiber bundle width. *PLoS One*. 2019;14:e0223350.
31. Scoles D, Gray DC, Hunter JJ, et al. In-vivo imaging of retinal nerve fiber layer vasculature: imaging histology comparison. *BMC Ophthalmol*. 2009;9:9.
32. Wells-Gray EM, Choi SS, Slabaugh M, Weber P, Doble N. Inner retinal changes in primary open-angle glaucoma

Investigative Ophthalmology & Visual Science

revealed through adaptive optics-optical coherence tomography. *J Glaucoma*. 2018;27:1025–1028.
33. Hasegawa T, Ooto S, Takayama K, et al. Cone integrity in glaucoma: an adaptive-optics scanning laser ophthalmoscopy study. *Am J Ophthalmol*. 2016;171:53–66.
34. Choi SS, Zawadzki RJ, Lim MC, et al. Evidence of outer retinal changes in glaucoma patients as revealed by ultrahigh-resolution in vivo retinal imaging. *Br J Ophthalmol*. 2011;95:131–141.
35. Rossi EA, Granger CE, Sharma R, et al. Imaging individual neurons in the retinal ganglion cell layer of the living eye. *Proc Natl Acad Sci USA*. 2017;114:586–591.
36. Liu Z, Kurokawa K, Zhang F, Lee JJ, Miller DT. Imaging and quantifying ganglion cells and other transparent neurons in the living human retina. *Proc Natl Acad Sci USA*. 2017;114:12803–12808.
37. Sharma R, Williams DR, Palczewska G, Palczewski K, Hunter JJ. Two-photon autofluorescence imaging reveals cellular structures throughout the retina of the living primate eye. *Invest Ophthalmol Vis Sci*. 2016;57:632–646.
38. Prum BE, Jr., Lim MC, Mansberger SL, et al. Primary open-angle glaucoma suspect preferred practice pattern guidelines. *Ophthalmology*. 2016;123:P112–P151.
39. Hodapp E, Parrish RK, Anderson DR. *Clinical decisions in glaucoma*. St. Louis*:* Mosby–YearBook; 1993:52–61.
40. Liu Z, Tam J, Saeedi O, Hammer DX. Trans-retinal cellular imaging with multimodal adaptive optics. *Biomed Opt Express*. 2018;9(9):4246–4262.
41. ANSI, Z136.1 –2014. *American National Standard for Safe Use of Lasers*. Orlando: Laser Institute of America; 2014.
42. Do NH. *Parallel processing for adaptive optics optical coherence tomography (AO-OCT) image registration using GPU* [master's thesis]. (Indianapolis: Indiana University–Purdue University Indianapolis; 2016.
43. Bennett AG, Rudnicka AR, Edgar DF. Improvements on Littmann's method of determining the size of retinal features by fundus photography. *Graefes Arch Clin Exp Ophthalmol*. 1994;232(6):361–367.
44. Curcio CA, Allen KA. Topography of ganglion cells in human retina. *J Comp Neurol*. 1990;300:5–25.
45. Heijl A, Patella V, Bengtsson B. *The Field Analyzer Primer: Effective Perimetry*. 4th Ed. Dublin, CA: Carl Zeiss Meditec; 2012.
46. Pazos M, Dyrda AA, Biarnes M, Gomez A, Martin C, Mora C, Fatti G, Anton A. Diagnostic Accuracy of Spectralis SD OCT Automated Macular Layers Segmentation to Discriminate Normal from Early Glaucomatous Eyes. *Ophthalmology*. 2017;124:1218–1228.
47. Watson AB. A formula for human retinal ganglion cell receptive field density as a function of visual field location. *J Vis*. 2014;14(7):15.
48. Stone J, Johnston E. The topography of primate retina: a study of the human, bushbaby, and new- and old-world monkeys. *J Comp Neurol*. 1981;196:205–223.
49. Blanks JC, Torigoe Y, Hinton DR, Blanks RH. Retinal pathology in Alzheimer's disease. I. Ganglion cell loss in foveal/parafoveal retina. *Neurobiol Aging*. 1996;17:377–384.
50. Rodieck RW, Binmoeller KF, Dineen J. Parasol and midget ganglion cells of the human retina. *J Comp Neurol*. 1985;233:115–132.
51. Pavlidis M, Stupp T, Hummeke M, Thanos S. Morphometric examination of human and monkey retinal ganglion cells within the papillomacular area. *Retina*. 2006;26:445–453.
52. McKendrick AM, Badcock DR, Morgan WH. Psychophysical measurement of neural adaptation abnormalities in magnocellular and parvocellular pathways in glaucoma. *Invest Ophthalmol Vis Sci*. 2004;45:1846–1853.
53. Soltanian-Zadeh S, Kurokawa K, Liu Z, Hammer DX, Miller DT, Farsiu S. Fully automatic quantification of individual ganglion cells from AO-OCT volumes via weakly supervised learning. *Ophthalmic Technologies XXX*. 2020;11218:112180Q.
54. Drasdo N, Millican CL, Katholi CR, Curcio CA. The length of Henle fibers in the human retina and a model of ganglion receptive field density in the visual field. *Vis Res*. 2007;47:2901–2911.
55. Bensinger E, Rinella N, Saud A, et al. Loss of foveal cone structure precedes loss of visual acuity in patients with rod-cone degeneration. *Invest Ophthalmol Vis Sci*. 2019;60(8):3187–3196.
56. Gardiner SK, Mansberger SL, Fortune B. Time lag between functional change and loss of retinal nerve fiber layer in glaucoma. *Invest Ophthalmol Vis Sci*. 2020;61(13):5–5.
57. Hammer DX, Liu Z, Cava JA, Carroll J, Saeedi O. On the axial location of Gunn's dots. *Am J Ophthalmol Case Rep*. 2020;19:100757.
58. Hammer DX, Villanueva R, Agrawal A, Saeedi O, Liu Z. Distribution of inner limiting membrane microglia in glaucoma measured with adaptive optics–optical coherence tomography. *Invest Ophthalmol Vis Sci*. 2020;61(7):3498.
59. Kurokawa K, Crowell JA, Zhang F, Miller DT. Suite of methods for assessing inner retinal temporal dynamics across spatial and temporal scales in the living human eye. *Neurophotonics*. 2020;7(1):015013.
60. Alberts B, Johnson A, Lewis J, Morgan D, Raff M, Roberts K. *Molecular Biology of the Cell. 6th ed*. New York: W. W. Norton & Company; 2014.
61. Cordeiro MF, Normando EM, Cardoso MJ, et al. Real-time imaging of single neuronal cell apoptosis in patients with glaucoma. *Brain*. 2017;140:1757–1767.
62. Dubin MW. The inner plexiform layer of the vertebrate retina: a quantitative and comparative electron microscopic analysis. *J Comp Neurol*. 1970;140:479–505.
63. Rathnasamy G, Foulds WS, Ling EA, Kaur C. Retinal microglia—A key player in healthy and diseased retina. *Prog Neurobiol*. 2019;173:18–40.
64. Distler C, Dreher Z. Glia cells of the monkey retina–II. Muller cells. *Vis Res*. 1996;36(16):2381–2394.
65. Franze K, Grosche J, Skatchkov SN, Schinkinger S, Foja C, Schild D, Uckermann O, Travis K, Reichenbach A, Guck J. Muller cells are living optical fibers in the vertebrate retina. *Proc Natl Acad Sci USA*. 2007;104(20):8287–8292.
66. Shou T, Liu J, Wang W, Zhou Y, Zhao K. Differential dendritic shrinkage of alpha and beta retinal ganglion cells in cats with chronic glaucoma. *Invest Ophthalmol Vis Sci*. 2003;44:3005–3010.
67. Feng L, Zhao Y, Yoshida M, et al. Sustained ocular hypertension induces dendritic degeneration of mouse retinal ganglion cells that depends on cell type and location. *Invest Ophthalmol Vis Sci*. 2013;54(2):1106–1117.
68. El-Danaf RN, Huberman AD. Characteristic patterns of dendritic remodeling in early-stage glaucoma: evidence from genetically identified retinal ganglion cell types. *J Neurosci*. 2015;35:2329–2343.
69. Risner ML, Pasini S, Cooper ML, Lambert WS, Calkins DJ. Axogenic mechanism enhances retinal ganglion cell excitability during early progression in glaucoma. *Proc Natl Acad Sci USA*. 2018;115:E2393–E2402.
70. Perez De Sevilla Muller L, Shelley J, Weiler R. Displaced amacrine cells of the mouse retina. *J Comp Neurol*. 2007;505:177–189.

Investigative Ophthalmology & Visual Science

71. Balendra SI, Normando EM, Bloom PA, Cordeiro MF. Advances in retinal ganglion cell imaging. *Eye (Lond)*. 2015;29:1260–1269.
72. Hammer DX, Agrawal A, Villanueva R, Saeedi O, Liu Z. Label-free adaptive optics imaging of human retinal macrophage distribution and dynamics. *Proc Natl Acad Sci USA*. 2020;117:30661–30669.
73. Silverman SM, Wong WT. Microglia in the retina: roles in development, maturity, and disease. *Ann Rev Vis Sci*. 2018;4:45–77.
74. Kocaoglu OP, Turner TL, Liu Z, Miller DT. Adaptive optics optical coherence tomography at 1 MHz. *Biomed Opt Express*. 2014;5:4186–4200.

Supplementary Material

Supplementary Video S1. Volumetric visualization of GCL somas in a representative AO-OCT volume from the right eye of a control subject (4136) at 12° temporal eccentricity. GCL soma center coordinates (*x, y, z*) were manually marked (blue crosses '+') using custom developed software which permits reliable cell identification through simultaneous visualization of B-scan cross-sections in both fast (A) and slow (B) directions and *en face* projection (C) at the depth-of-interest. Red lines indicate locations in the corresponding planes. Scalebar = 100 µm.

Supplementary Video S2. Representative 3D volumetric visualization of 12°(L5) data set from the left eye of a 51-year-old glaucoma patient (1733) with superior HD. AO-OCT revealed a significant decrease in GCL soma density and increase in GCL soma diameter. *En face* fly-through image was projected at the depth indicated by the white arrow in the B-scan view. Scalebar = 50 µm.

Supplementary Video S3. AO-OCT revealed retinal tissue re-modeling in the IPL that was possibly related to glaucoma. Example of hyper reflective structures (e.g. blue arrow in frame 43-58) observed in the defective hemifield (inferior retina) in the right eye of a 62-year-old glaucoma patient (1541, data were taken at location L2). *En face* fly-through image was projected at the depth indicated by the white arrow in the B-scan view. A hypo-reflective region indicated as pink arrow (frame 106–130) was also observed in the INL, which is likely a microcytic lesion. Scalebar = 50 µm.

Investigative Ophthalmology & Visual Science